Limit of Metastability for Liquid and Vapor Phases of Water

Woo Jong Cho,[1,2] Jaegil Kim,[3] Joonho Lee,[2] Thomas Keyes,[4] John E. Straub,[4] and Kwang S. Kim[1,*]
[1]Department of Chemistry, Ulsan National Institute of Science and Technology (UNIST), Ulsan 689-798, Korea
[2]Department of Chemistry, Pohang University of Science and Technology, Pohang 790-784, Korea
[3]Broad Institute of MIT and Harvard, Cambridge, Massachusetts 02142, USA
[4]Department of Chemistry, Boston University, Boston, Massachusetts 02215, USA
(Received 14 September 2013; published 16 April 2014)

We report the limits of superheating of water and supercooling of vapor from Monte Carlo simulations using microscopic models with configurational enthalpy as the order parameter. The superheating limit is well reproduced. The vapor is predicted to undergo spinodal decomposition at a temperature of $T_{\mathrm{sp}}^{\mathrm{vap}} = 46 \pm 10\,^{\circ}\mathrm{C}$ ($0\,^{\circ}\mathrm{C} \ll T_{\mathrm{sp}}^{\mathrm{vap}} \ll 100\,^{\circ}\mathrm{C}$) under 1 atm. The water-water network begins to form at the supercooling limit of the vapor. Three-dimensional water-water and cavity-cavity unbroken networks are interwoven at critically superheated liquid water; if either network breaks, the metastable state changes to liquid or vapor.

DOI: 10.1103/PhysRevLett.112.157802 PACS numbers: 61.20.Ja, 64.60.Q–, 64.70.F–

Water is presumably the most used and the most studied substance among all the chemicals known to mankind. In particular, scientists have been attracted to the diverse structures of water clusters, liquid, and ice resulting from different orientations of hydrogen bonds and the associated phenomena [1–14]. However, the liquid-vapor transition of water has been a subject of less intense investigation [15,16] because of difficulties in both experiment and computation due to the complicated metastable states separating the liquid and vapor phases. Given that everyday life experiences water evaporation and dew drops, it is ironic that these physical or chemical phenomena are not adequately understood. Simply, we are familiar with the generally learned fact that water boils at 100 °C or 373 K at 1 atm. However, water can be superheated up to 603 K at 1 atm, and water vapor can be supercooled considerably below the boiling point [17–21] though the limit of supercooling is not known yet. This is due to unfavorable energetics at the formation of the liquid-vapor interface, which allow for the temporary existence of metastable states. According to the classical nucleation theory, the metastable states can be kept stable until stochastic fluctuations create the so-called critical cluster, which then grows spontaneously to make a new phase [22].

However, these metastable states cease to exist when the liquid or vapor is brought to its stability limit, or spinodal. In this case, where the mother phase completely loses its thermodynamic stability, the phase transition takes place via spinodal decomposition [23]. It differs from classical nucleation in which the phase transition takes place at localized regions of space. Instead, the phase transition is considered to proceed by merging small embryos of daughter phase distributed uniformly over the space [24]. The lifetime of systems near the stability limit is too short to allow for accurate experimental determination of the spinodal. Hence, predicting the stability limit from a microscopic model of matter is of immense importance, given that there are a plethora of phenomena depending on the metastability throughout biology, meteorology, and industry [22].

In this Letter, based on targeted sampling of metastable and unstable states which are inaccessible to ordinary Monte Carlo simulations, with the choice of configurational enthalpy as the order parameter, for the first time, we report the limits of metastable states, or spinodals, obtained from microscopic models of water. The liquid can be heated up to the liquid spinodal temperature without losing the connectedness among water molecules while forming a full space-spanning connected network of cavity space arising from density fluctuations. On the other hand, at the vapor spinodal temperature (the minimum temperature to which the metastable vapor phase extends), the water-water network of small liquid clusters (i.e., clusterization) just starts to develop in the vapor.

To this end, using the generalized replica exchange method (GREM) [25,26], we have performed umbrella sampling for a number of enthalpy windows, with a thermometer in each window. The average temperature T_S, thus measured, as a function of configurational enthalpy H and pressure p in the isobaric-isenthalpic ensemble, is the statistical temperature $T_S(H;p) \equiv (\partial S/\partial H)_p^{-1}$, which is a system's intrinsic property. The entropy $S(H;p)$ in this ensemble is expressed as

$$S(H;p) = k_B \ln \int dV d\mathbf{x}^N \delta(H - E(\mathbf{x}^N) - pV), \quad (1)$$

where V is the volume, $\mathbf{x}^N$ is a possible configuration of N molecules, and k_B is the Boltzmann constant. The stability condition $(\partial^2 S/\partial H^2)_p < 0$ is equivalent to $(\partial T_S/\partial H)_p > 0$.

Therefore, the liquid and vapor spinodals are located on the points where $(\partial T_S/\partial H)_p$ changes the sign.

TIP4P-like models, which regard a water molecule as the collection of a Lennard-Jones particle and three point charges, are known to reproduce the condensed phases of water with reasonable accuracy [27]. For the study of liquid-vapor transition, we choose the TIP4P model [28] which gives the best estimate of vapor pressure [29] among its kind. The statistical temperature $T_S(H;p)$ of TIP4P water at various external pressures is given in Fig. 1(a). Each curve comprises two stable branches with positive slopes which correspond to homogeneous liquid and gas phases, and an unstable branch with a negative slope. The maximum and minimum in each curve correspond to the liquid and vapor spinodals, respectively. The extrema merge to become the inflection point at the critical pressure and temperature above which the distinction of liquid and vapor phases no longer exist. In our calculations, such a behavior appears for the external pressure of 150 atm at 583 K, as compared to the experimental value of 218 atm and 647 K.

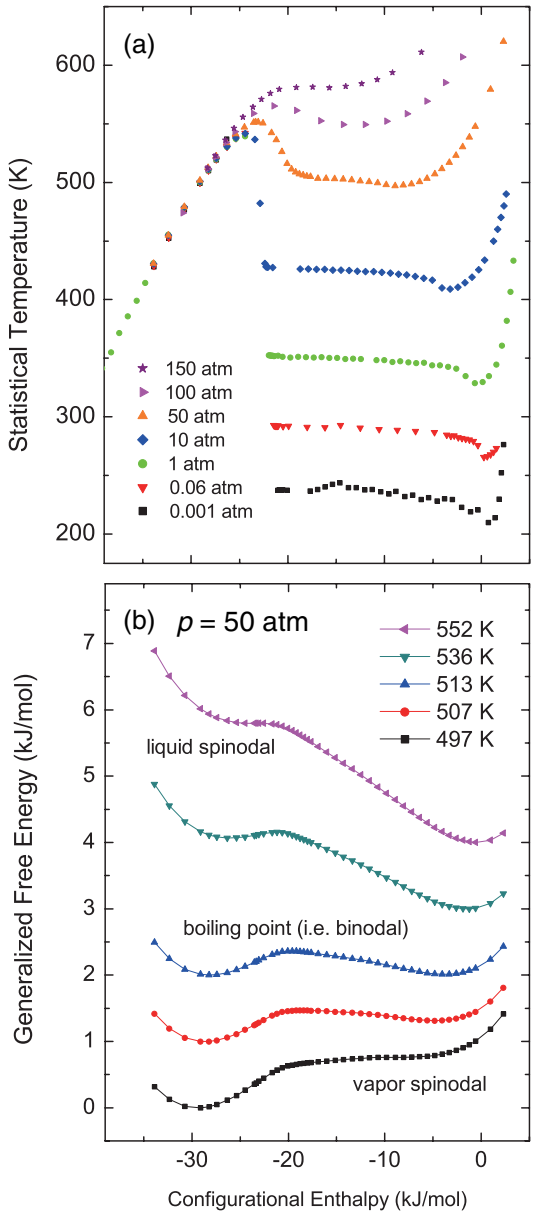

FIG. 1 (color online). (a) Calculated statistical temperatures of 512 TIP4P water molecules at various external pressures. (b) Generalized free energy $F(H;T,p)$ calculated using Eq. (3) at $p = 50$ atm and the specified temperatures. Offsets are applied for the sake of clarity without loss of physical meaning.

The configurational enthalpy H (in contrast to the system's enthalpy as a thermodynamic average) represents the instantaneous value of the enthalpy function $H(\mathbf{x}^N, V) = E(\mathbf{x}^N) + pV$, which fluctuates around its average. The fluctuation of H in the isobaric-isothermal ensemble is described by the generalized free energy $F(H;T,p)$

$$-\beta F(H;T,p) \equiv \ln \int dV d\mathbf{x}^N e^{-\beta H} \delta(H - E(\mathbf{x}^N) - pV). \tag{2}$$

Comparing Eq. (1) and Eq. (2), $F(H;T,p)$ can be evaluated up to an additive constant in an indirect manner using the statistical temperature $T_S(H;p)$ obtained from the GREM simulation

$$F(H;T,p) = H - T \int^H \frac{dH'}{T_S(H';p)}. \tag{3}$$

Plots of this quantity at various temperatures under $p =$ 50 atm are shown in Fig. 1(b). Between the liquid and vapor spinodals, the generalized free energy has two minima corresponding to the (meta)stable liquid and vapor states. However, one of the two minima disappears to become an inflection point at the liquid and vapor spinodals. Therefore, a phase at its spinodal point makes the transition to the other phase under an infinitesimal perturbation.

The liquid spinodal is only weakly dependent on the external pressure, as can be expected from its low compressibility compared to the gas phase. The TIP4P water can withstand a temperature up to 542 K under 1 atm, within 10% error from the experimental superheating limit 603 K. The TIP4P/2005 model [27], which is specialized only for the use in condensed phases [29,30], gives a superheating limit of 601 K under 1 atm. This indicates that the liquid spinodal is determined mainly by liquid state properties, not by relative stability of liquid and vapor states.

The superheated water near the liquid spinodal undergoes spontaneous cavitation and subsequent phase transition to vapor. However, the complete sampling of bubble-in-liquid configurations would require a simulation with an impractically large number of molecules [31,32]. This problem can be avoided when the external pressure is high so that the bubbles are small enough to fit in the simulation cell. This suppression of finite size effect is the

reason why smooth statistical temperature curves appear at high pressures. The average density of critically superheated water at 1 atm is found to be about 0.5 g/cm^3. This decrease in density can be explained by the frequent intervention of cavities in the liquid structure, as can be confirmed by the radial distribution function (RDF) and the substantial fluctuation (see the Supplemental Material [33]). The RDF shows that the long-range order is almost smeared out in the superheated water as compared to water at ambient conditions. The fluctuation analysis reveals that cavities as large as 10 Å in diameter form occasionally.

However, the above analysis of the cavity space is rather indirect. To quantify the network of cavity space appearing within the sampled configurations, we coarse-grained the simulation cell into small cubes of liquid and cavity. Clustering of neighboring points is performed, and the connectivity p_c, defined in Eq. (4), is calculated for each liquid and cavity lattice

$$p_c \equiv \frac{1}{N^2}\sum_{i=1}^{N} i^2 n_i, \tag{4}$$

where N, i, and n_i are the total number of liquid or cavity lattice points, cluster size, and number of i-sized clusters, respectively. It is defined in such a way that big clusters contribute more to the connectivity. The ensemble average of connectivities of liquid and cavity lattices are calculated for coarse-grained configurations generated from the simulation at 50 atm. Figure 2 shows the average connectivity

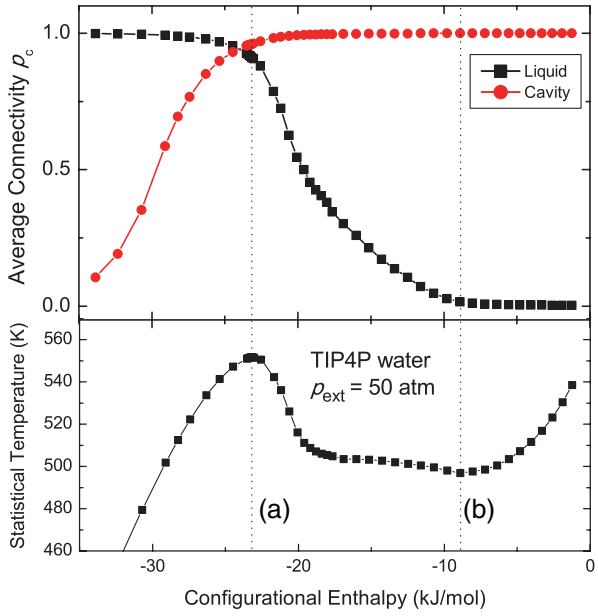

FIG. 2 (color online). The connectivity index p_c is averaged over 10 000 coarse-grained configurations obtained from the simulation of 512 TIP4P waters under 50 atm. The vertical dotted lines represent (a) liquid at liquid spinodal temperature and (b) vapor at vapor spinodal temperature.

of liquid and cavity as the system is moved along the statistical temperature curve. The liquid spinodal can be understood as the point from which the network of liquid water starts to fragment into many pieces. The thermodynamic stability of water terminates at the liquid spinodal. Approaching from the vapor side, the vapor spinodal can be understood as the point where the recovery of liquid connectivity begins, consistent with the traditional thermodynamic argument.

Since the vapor spinodal is experimentally unknown, we attempt to find the upper and lower bounds using two different water models, namely the TIP4P and Matsuoka-Clementi-Yoshimine (MCY) [44] models. The TIP4P model is fitted to the liquid phase, and thus exaggerates the dipole moment (2.18 D) from its gas-phase value 1.86 D [45]. On the other hand, the MCY model is fitted to the *ab initio* potential energy surface of water dimer. Therefore, it has a tendency to underestimate the binding energy of a cluster [46]. On this ground, another set of GREM simulations is performed to obtain the vapor spinodal temperatures of the MCY model in a wide range of external pressure. The calculated vapor spinodal of TIP4P and MCY models are shown in Fig. 3(a), where it can be seen that, upon isobaric cooling, the TIP4P vapor undergoes spinodal decomposition earlier (i.e., at higher temperature) than MCY vapor does. The critical supersaturation ratio to induce spinodal decomposition is calculated from the simulated vapor spinodals and the experimental vapor pressure of water, and shown in the inset of Fig. 3(a). Here, we expect that the true vapor spinodal of water lies in between that of TIP4P and MCY models, since the system is composed of small and intermediate-sized clusters as shown in Fig. 3(b). For example, water vapor at 1.0 atm (equilibrium vapor pressure at 100 °C) undergoes spinodal decomposition when supercooled to 46±10°C (319 ± 10 K). Currently, available experimental data [20,21] on the nucleation rate of supersaturated vapor do not cover the supersaturation range where the spinodal decomposition is predicted to occur.

Now, we turn our attention on the cluster distribution of different enthalpy windows. The average mass fraction of i-sized clusters f_i is calculated in Fig. 3(b) using the definition $f_i \equiv in_i/N$ where N is the total number of molecules, i is the cluster size, and n_i is the number of i-sized clusters. The cluster fraction has a peak for low-enthalpy ensembles, and this peak broadens as the system is moved to high enthalpies, until it disappears at the vapor spinodal. This can be regarded as the transition from classical nucleation to the spinodal decomposition. We note that the critical nucleus does not diverge at the spinodal, consistent with the previous experimental findings [47].

The process of liquid-vapor phase transition can be visualized by showing representative snapshots of configurations along the statistical temperature curve (Fig. 4).

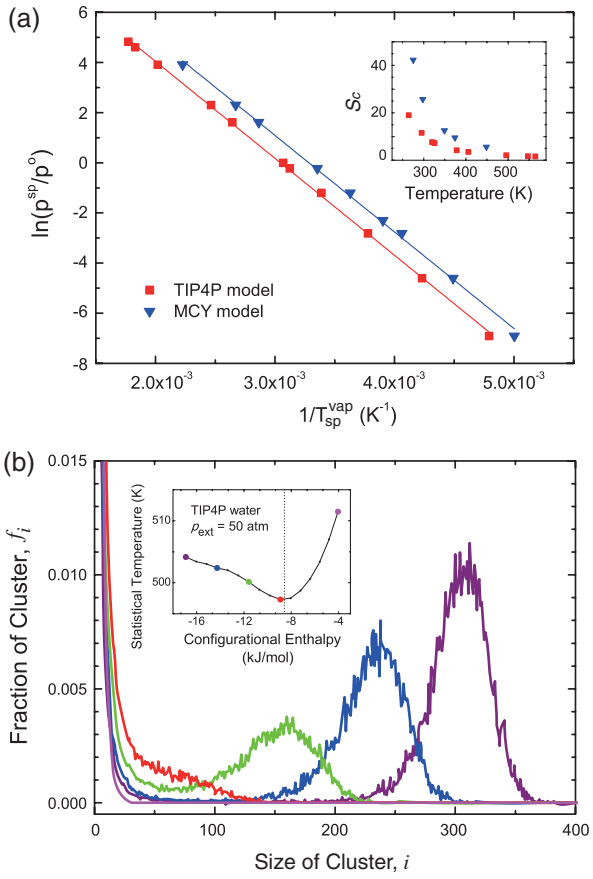

FIG. 3 (color online). (a) Vapor spinodal temperatures $T_{\mathrm{sp}}^{\mathrm{vap}}$ under the pressure p^{sp} for TIP4P and MCY models. The reference pressure $p^\circ = 1$ atm. Inset: The critical supersaturation ratio $S_c = p^{\mathrm{sp}}/p^{\mathrm{sat}}$ calculated at each data point, where equilibrium vapor pressure p^{sat} is obtained from the steam table [48]. (b) The average fraction $f_i = in_i/N$ of i-sized clusters at each colored point marked on the statistical temperature curve (inset). Inset: the statistical temperature curve near the vapor spinodal (vertical dotted line).

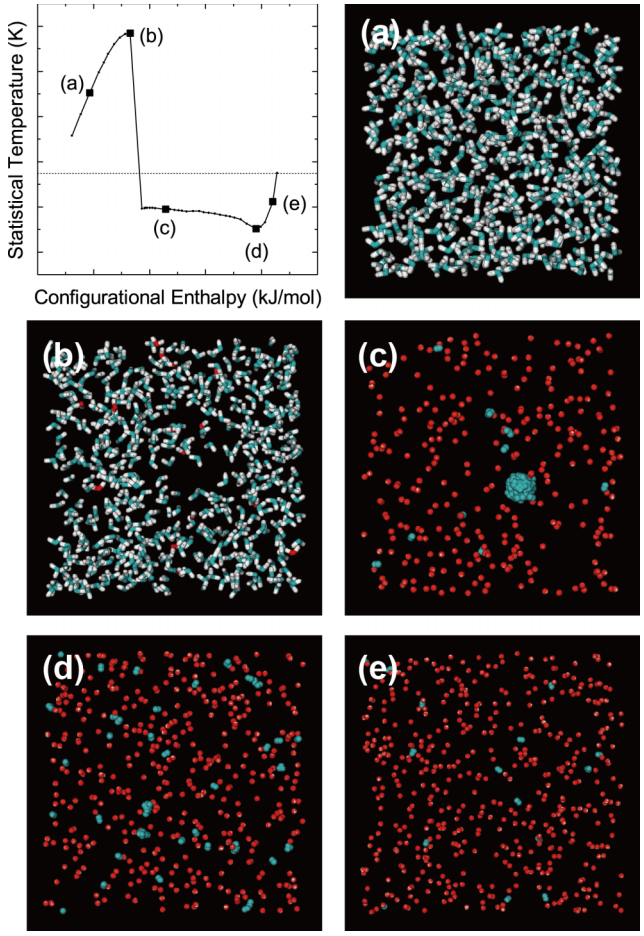

FIG. 4 (color online). The equilibrium boiling point T_b is marked with a horizontal dotted line on the plot of statistical temperature. The snapshots represent (a) metastable liquid above the boiling point, (b) liquid at liquid spinodal, (c) classical nucleation regime, (d) vapor at vapor spinodal, and (e) metastable supersaturated vapor. The Stillinger clusters [49] with cutoff radius $r_c = 3.375$ Å are identified and colored light gray (cyan). Gaslike molecules are dark gray (red). The configurations are generated from the simulation of 512 TIP4P waters under the external pressure of 1 atm.

Away from the liquid spinodal, yet above the boiling point, superheated liquid water maintains the homogeneity. The homogeneity is lost as we approach the liquid spinodal where the cavity has grown to a considerable size. Likewise, the vapor phase can be cooled down to the vapor spinodal much below the boiling point while keeping the homogeneity intact. The vapor to liquid transition of this metastable vapor is governed by classical nucleation whose prerequisite is the stochastic formation of critical nucleus shown in Fig. 4(c). However, when the supercooling is deep enough to reach the vapor spinodal, the phase transition is initiated from the small clusters shown in Fig. 4(d).

Thus far, we reproduced the experimental superheating limit of the liquid water, and predicted the supercooling limit of the water vapor by performing Monte Carlo simulations using microscopic models of the water molecule. As the liquid is heated, cavities arising from natural density fluctuations within the liquid start to form a network. At the liquid spinodal, the cavity networking is complete and three-dimensional water-water and cavity-cavity fully connected networks are interpenetrated. As the water or cavity network breaks, the state changes to vapor or liquid. The simple classical nucleation model does not capture this weblike cavity within the liquid. On the other hand, as the vapor is cooled down to the vapor spinodal temperature, the water molecules start to aggregate. This aggregation is dispersed uniformly in the space, and differs from the classical nucleation which is valid for low supersaturations. Understanding the intriguing vapor-liquid transition phenomena is directly related to the microwave superheating accidents of water and, furthermore, could be utilized to harvest water in extreme conditions such as dry

areas by optimizing the liquid-vapor transition in ingenuously designed confined or interface systems.

K. S. K. acknowledges support by NRF (National Honor Scientist Program, No. 2010-0020414) and KISTI (No. KSC-2011-G3-02). J. E. S. acknowledges the support of the National Science Foundation (No. CHE-1114676).

*Corresponding author.
kimks@unist.ac.kr

[1] C. Pérez, M. T. Muckle, D. P. Zaleski, N. A. Seifert, B. Temelso, G. C. Shields, Z. Kisiel, and B. H. Pate, Science **336**, 897 (2012).
[2] H. M. Lee, S. B. Suh, J. Y. Lee, P. Tarakeshwar, and K. S. Kim, J. Chem. Phys. **112**, 9759 (2000).
[3] N. J. Singh, M. Park, S. K. Min, S. B. Suh, and K. S. Kim, Angew. Chem., Int. Ed. **45**, 3795 (2006).
[4] J. R. R. Verlet, A. E. Bragg, A. Kammrath, O. Cheshnovsky, and D. M. Neumark, Science **307**, 93 (2005).
[5] K. S. Kim, I. Park, S. Lee, K. Cho, J. Y. Lee, J. Kim, and J. D. Joannopoulos, Phys. Rev. Lett. **76**, 956 (1996).
[6] M. E. Tuckerman, D. Marx, and M. Parrinello, Nature (London) **417**, 925 (2002).
[7] P. L. Geissler, C. Dellago, D. Chandler, J. Hutter, and M. Parrinello, Science **291**, 2121 (2001).
[8] T. D. Kühne and R. Z. Khaliullin, Nat. Commun. **4**, 1450 (2013).
[9] O. Mishima and H. E. Stanley, Nature (London) **396**, 329 (1998).
[10] I. Park, K. Cho, S. Lee, K. S. Kim, and J. D. Joannopoulos, Comput. Mater. Sci. **21**, 291 (2001).
[11] M. Matsumoto, S. Saito, and I. Ohmine, Nature (London) **416**, 409 (2002).
[12] E. B. Moore and V. Molinero, Nature (London) **479**, 506 (2011).
[13] J. R. Errington, P. G. Debenedetti, and S. Torquato, Phys. Rev. Lett. **89**, 215503 (2002).
[14] M. Sharma, R. Resta, and R. Car, Phys. Rev. Lett. **98**, 247401 (2007).
[15] I. F. W. Kuo and C. J. Mundy, Science **303**, 658 (2004).
[16] D. Zahn, Phys. Rev. Lett. **93**, 227801 (2004).
[17] R. A. Apfel, Nature (London) **238**, 63 (1972).
[18] R. J. Speedy, J. Phys. Chem. **86**, 982 (1982).
[19] M. T. Carlson, A. J. Green, and H. H. Richardson, Nano Lett. **12**, 1534 (2012).
[20] Y. Viisanen, R. Strey, and H. Reiss, J. Chem. Phys. **99**, 4680 (1993).
[21] D. Brus, V. Zdímal, and H. Uchtmann, J. Chem. Phys. **131**, 074507 (2009).
[22] P. G. Debenedetti, *Metastable Liquids: Concepts and Principles* (Princeton University Press, Princeton, NJ, 1996).
[23] J. W. Cahn, J. Chem. Phys. **42**, 93 (1965).
[24] P. Bhimalapuram, S. Chakrabarty, and B. Bagchi, Phys. Rev. Lett. **98**, 206104 (2007).
[25] J. Kim, T. Keyes, and J. E. Straub, J. Chem. Phys. **132**, 224107 (2010).
[26] Q. Lu, J. Kim, and J. E. Straub, J. Chem. Phys. **138**, 104119 (2013).
[27] J. L. F. Abascal and C. Vega, J. Chem. Phys. **123**, 234505 (2005).
[28] W. L. Jorgensen, J. Chandrasekhar, J. D. Madura, R. W. Impey, and M. L. Klein, J. Chem. Phys. **79**, 926 (1983).
[29] C. Vega, J. L. F. Abascal, and I. Nezbeda, J. Chem. Phys. **125**, 034503 (2006).
[30] A. Pérez and A. Rubio, J. Chem. Phys. **135**, 244505 (2011).
[31] V. K. Shen and P. G. Debenedetti, J. Chem. Phys. **111**, 3581 (1999).
[32] C. Vega and E. de Miguel, J. Chem. Phys. **126**, 154707 (2007).
[33] See Supplemental Material, which includes Refs. [34–43], at http://link.aps.org/supplemental/10.1103/PhysRevLett.112.157802 for the RDF and number fluctuation shown in Fig. S1.
[34] D. J. Wales and M. P. Hodges, Chem. Phys. Lett. **286**, 65 (1998).
[35] T. James, D. J. Wales, and J. Hernndez-Rojas, Chem. Phys. Lett. **415**, 302 (2005).
[36] J. Pillardy, K. A. Olszewski, and L. Piela, J. Mol. Struct. **270**, 277 (1992).
[37] F. N. Keutsch, J. D. Cruzan, and R. J. Saykally, Chem. Rev. **103**, 2533 (2003).
[38] K. Kim, M. Dupuis, G. Lie, and E. Clementi, Chem. Phys. Lett. **131**, 451 (1986).
[39] S. S. Xantheas, C. J. Burnham, and R. J. Harrison, J. Chem. Phys. **116**, 1493 (2002).
[40] Y. Wang, B. C. Shepler, B. J. Braams, and J. M. Bowman, J. Chem. Phys. **131**, 054511 (2009).
[41] J. A. Anderson, K. Crager, L. Fedoroff, and G. S. Tschumper, J. Chem. Phys. **121**, 11023 (2004).
[42] B. Temelso, K. A. Archer, and G. C. Shields, J. Phys. Chem. A **115**, 12034 (2011).
[43] D. M. Bates and G. S. Tschumper, J. Phys. Chem. A **113**, 3555 (2009).
[44] O. Matsuoka, E. Clementi, and M. Yoshimine, J. Chem. Phys. **64**, 1351 (1976).
[45] P. L. Silvestrelli and M. Parrinello, Phys. Rev. Lett. **82**, 3308 (1999).
[46] B. J. Mhin, J. Kim, S. Lee, J. Y. Lee, and K. S. Kim, J. Chem. Phys. **100**, 4484 (1994).
[47] P. Debenedetti, Nature (London) **441**, 168 (2006).
[48] L. Haar, J. S. Gallagher, and G. S. Kell, *NBS/NRC Steam Tables* (Hemisphere, New York, 1984).
[49] F. H. Stillinger, Jr., J. Chem. Phys. **38**, 1486 (1963).